Author's personal copy

Applied Catalysis A: General 393 (2011) 29–35

Contents lists available at ScienceDirect

Applied Catalysis A: General

journal homepage: www.elsevier.com/locate/apcata

Cleavage of the C–O–C bond on size-selected subnanometer cobalt catalysts and on ALD-cobalt coated nanoporous membranes

Weiling Deng[a,1], Sungsik Lee[b,1], Joseph A. Libera[c], Jeffrey W. Elam[c], Stefan Vajda[d,e,f,*], Christopher L. Marshall[a,**]

[a] Chemical Sciences and Engineering Division, Argonne National Laboratory, United States
[b] X-ray Sciences Division, Argonne National Laboratory, United States
[c] Energy Systems Division, Argonne National Laboratory, United States
[d] Material Sciences Division, Argonne National Laboratory, United States
[e] Center for Nanoscale Materials, Argonne National Laboratory, Argonne, IL 60439, United States
[f] Department of Chemical Engineering, School of Engineering & Applied Science, Yale University, New Haven, CT 06511, United States

ARTICLE INFO

Article history:
Received 30 August 2010
Received in revised form 9 November 2010
Accepted 10 November 2010
Available online 18 November 2010

Keywords:
Oxidative decomposition
Cellulose
C–O–C bond cleavage
Size-selected clusters
Cobalt
Anodized aluminum oxide
Atomic layer deposition

ABSTRACT

The cleavage of the C–O–C bond was studied under oxidizing conditions on nanostructured membrane supported cobalt-based catalysts using a cellulose model surrogate, 1-methoxy-2-methyl-2-propanol. The cobalt catalysts were found to break the C–O–C bond, producing alcohols and/or ketones by further oxidation. The size-selected sub-nanometer size cobalt clusters exhibited a per metal activity of up to 5 orders of magnitude higher than the with atomic layer deposition uniformly coated membranes. The large difference in activity is attributed to the high fraction of the surface atoms of the subnanometer clusters. The positioning of the clusters at the entrance vs. exit of the catalytic membrane allows for a control of the contact time and consequently of the selectivity of the catalyst.

Published by Elsevier B.V.

1. Introduction

Renewable biofuels produced by catalytic breakdown of biomass such as cellulose has recently attracted increasing attention [1–3]. Cellulose is a polymer composed of hundreds to thousands of glucose monomer units, linked together by beta-(1,4)-glycosidic bonds, which is hard to degrade due to its robust crystal structure and its insolubility in water or conventional organic solvents. There are several processes reported in the literature on the breakdown of cellulose, such as acid hydrolysis using mineral acids [4,5], enzymatic hydrolysis [6–8], gasification [9], and reductive hydrolysis by precious metals under high pressure conditions [3]. The disadvantages of these processes include large amount of acidic waste, high energy input and low selectivity towards the desired products.

C–O–C bond cleavage in ethers has been reported by Gopinath et al. [10] in a liquid system on treatment with a catalytic quantity of V_2O_5 and H_2O_2 in methanol, in which tetrahydropyranyl and *tert*-butyldimethylsilyl ethers were cleaved regenerating the corresponding alcohols. Kinetics study and light-off experiment are not easy to carry out with this batch reactor liquid system. Our approach is to conduct gas (reactant)–solid (catalyst) reaction for the fast catalyst screening purpose. Reactions can be carried out at a temperature ramping mode to monitor the catalyst activity changes for the C–O–C bond cleavage.

This paper focuses on the selective oxidative cleavage of the C–O–C bond connecting adjacent glucose moieties in cellulose using a model surrogate compound 1-methoxy-2-methyl-2-propanol (MMP). The advantage of this compound is that it mimics the characteristic of the glycosidic bond in cellulose and can be readily transferred into the gas phase for reactivity studies under heterogeneous catalytic conditions. The goal of this study is to identify catalyst compositions and reaction conditions for highly active C–O–C bond breaking, while minimizing the breakage of

* Corresponding author at: Material Sciences Division and Center for Nanoscale Materials, Argonne National Laboratory, 9700 South Cass Avenue, MSD/200, Argonne, IL 60439-4831, United States. Tel.: +1 630 252 8123.
** Corresponding author at: Argonne National Laboratory, Chemical Science and Engineering Division, 9700 South Cass Avenue, CSE/205, Argonne, IL 60439-4831, United States. Tel.: +1 630 252 4310.
E-mail addresses: vajda@anl.gov (S. Vajda), marshall@anl.gov (C.L. Marshall).
[1] These two authors contributed equally to this work.

0926-860X/$ – see front matter. Published by Elsevier B.V.
doi:10.1016/j.apcata.2010.11.022

Author's personal copy

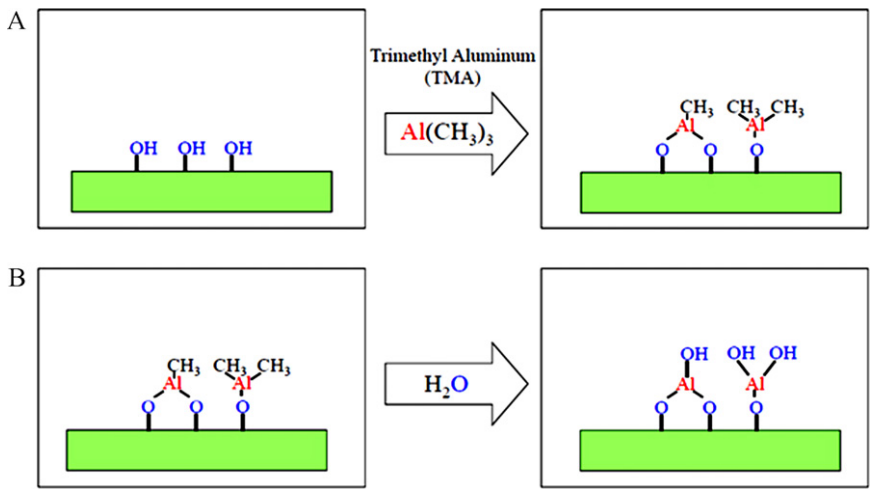

Fig. 1. Schematic illustration of Al_2O_3 ALD. Trimethyl aluminum (TMA) reacts with surface hydroxyls in step A yielding a methyl-terminated aluminum monolayer and CH_4 gas. During step B, this new surface is reacted with H_2O vapor resulting in the formation of a monolayer of Al_2O_3 and restoring the surface hydroxyl coverage.

non-glycosidic bonds, such as the C–C and C–OH bonds as well as the C–O–C bond inside the glucose ring.

The catalyst size dependent activity and selectivity is very important for a large variety of reactions [11]. For example, titania-supported gold nanoparticles of about 3 nm in size were found to be highly efficient catalysts for CO oxidation [12]; in steam reforming of CH_4 the C–H bond activation turnover rates increased with decreasing Pt cluster size (2–6 nm) [13]. Bus et al. showed that gold clusters with a diameter below 2 nm are essential to obtain a high activity and selectivity in the high-pressure liquid-phase hydrogenation of cinnamaldehyde [14].

Catalysts prepared by conventional techniques such as incipient wetness impregnation, and deposition–precipitation typically incorporate a wide range of various particle sizes. Underlying atomic-scale metal clusters are not easy to characterize and it is very difficult to separate the function of those clusters from the nanosized particles in reactions [15,16]. Using a size-selected cluster deposition method, precise control of metal cluster size can be achieved. Size-selected clusters have shown high reactivity in various reactions, such as supported Au and Pd clusters in CO oxidation [17–20] under ultra-high vacuum (UHV) conditions, free Ag and Au clusters in CO oxidation [21–23] or free $V_xO_y^+$ gas clusters in the reactions with hydrocarbons [24]. Recently, size-preselected sub-nanometer Pt and clusters supported on amorphous supports were found highly active and selective in the oxidative dehydrogenation of propane [25], sub-nanometer Au and sub-nanometer

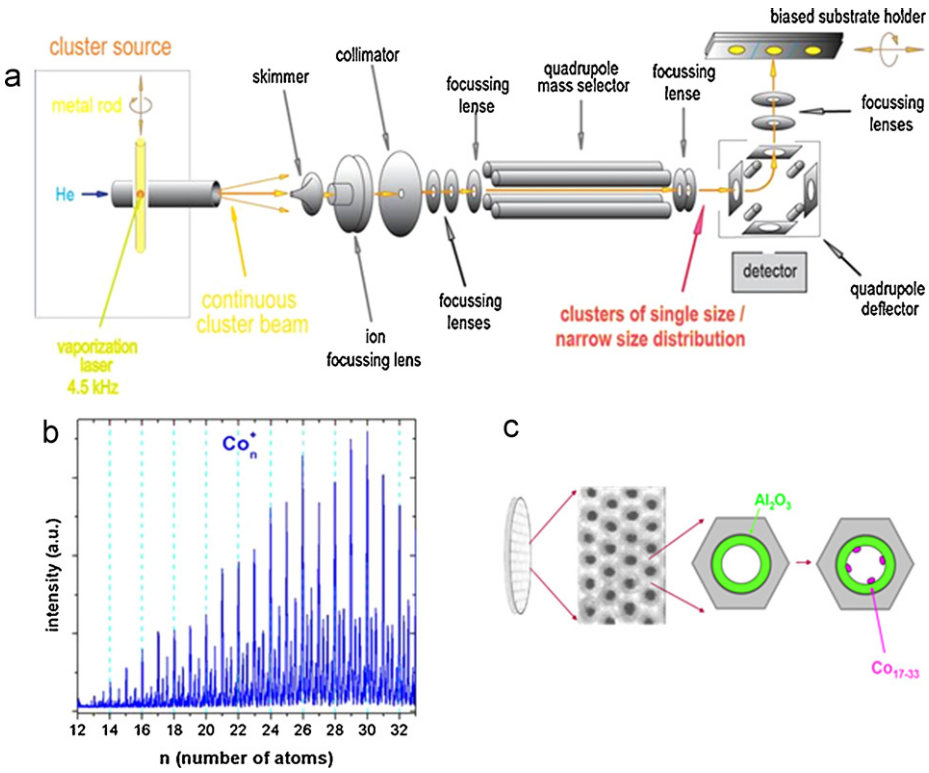

Fig. 2. Schematics of the cluster deposition apparatus (a) mass spectrum of the deposited distribution of cobalt clusters showing a fraction of partially oxidized clusters under vacuum conditions. After exposure to air, the clusters become oxidized as determined by XANES (b), and cartoon of the $Co_{17-33}/Al_2O_3/ZnO/Al_2O_3$/AAO sample (c).

Author's personal copy

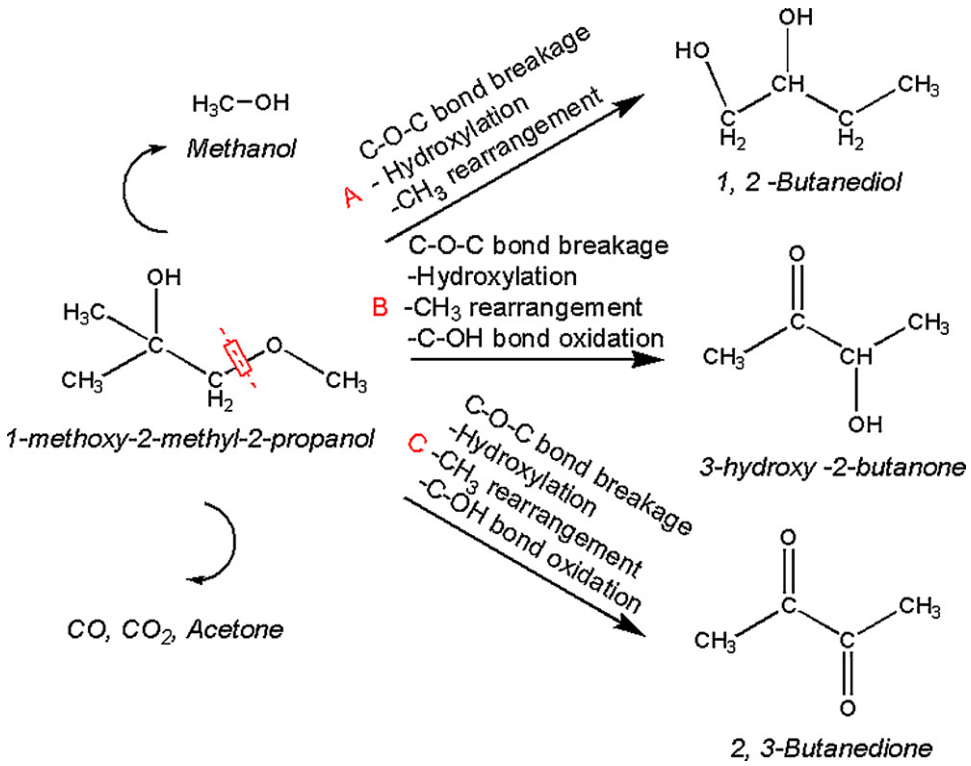

Fig. 3. Schematics of reaction pathways for the oxidative decomposition of 1-methoxy-2-methyl-2-propanol (MMP).

to nanometer size-selected Ag clusters in the partial oxidation of alkenes [26–29], and sub-nm Pd clusters in oxidative activation of methanol [30] under realistic reaction conditions.

The focus of the presented study is to investigate the selectivity and reactivity of two types of cobalt species supported on nanoporous anodized aluminum oxide (AAO) membranes: (1) size preselected subnanometer cobalt clusters and (2) cobalt-oxide coating prepared by atomic layer deposition (ALD). The well defined location of the size-selected clusters on the AAO support moreover allows for straightforward studies of the effect of contact time on catalyst performance as well.

2. Experimental

2.1. Catalyst support preparation

As catalyst support, high surface area nanoporous AAO membranes with a pore diameter of 40 nm, at 16% of surface pore openings were prepared in our lab. 40 nm pores were selected since this pore size yields the most well-ordered AAO membranes. The membrane thickness is 70 μm. The circular membranes had an integral aluminum ring around the perimeter allowing for a tight mount in the test reactor. Prior to the ALD coatings, the AAO membranes were allowed to outgas in 360 sccm of ultrahigh purity (UHP) nitrogen at 1 Torr and 200 °C for 10 min. Next, the AAO membranes were cleaned using a 5 min exposure to 400 sccm of 10% ozone in oxygen.

The membranes were coated by ALD at a temperature of 200 °C in a viscous flow reactor (see Fig. 1) [31]. First, a 1 nm Al_2O_3 coating was applied on the AAO membranes using 10 ALD cycles consisting of alternating exposures to trimethyl aluminum and water to result in a chemically uniform alumina surface by covering the aluminum oxalate residues from AAO membrane production. Step A in Fig. 1 is the introduction of trimethyl-aluminum to react with surface hydroxyl groups on the membrane support, yielding a methyl-terminated aluminum monolayer and methane gas. During step B, this new surface is reacted with H_2O vapor resulting in the formation of a monolayer of Al_2O_3 and restoring the surface hydroxyl coverage. Repeating this binary reaction sequence in an ABAB... fashion yields Al_2O_3 growth at a rate of 0.12 nm per AB cycle. The ALD cobalt oxide catalysts were applied directly on the top of this Al_2O_3 layer.

For the cluster deposition, the membranes were manufactured by adding (1) a 2 nm ZnO coating using 10 ALD cycles consisting of alternating exposures to diethyl zinc and water followed by (2) a 1 nm Al_2O_3 coating. The electrically conducting ZnO film of the Al_2O_3/ZnO/Al_2O_3 multilayer facilitated an exact determination of ultra-small metal loadings during size-selected cluster deposition. The final 1 nm Al_2O_3 layer ensures that the surface chemistry of the support for the cluster deposited cobalt oxide is identical to that of the ALD cobalt oxide samples.

2.2. Catalyst deposition

The ALD-based cobalt oxide sample (ALD-CoO/Al_2O_3/AAO) was prepared at a temperature of 465 °C using one ALD cycle consisting of a 500 s exposure to bis(cyclopentadienyl) cobalt at a partial pressure of 10 mTorr followed by a 100 s purge during which only the UHP nitrogen was flowing, and ending with a 500 s exposure to ozone at a partial pressure of 100 mTorr. Mass spectrometric analysis of the gas-phase reaction products shows only CO_2 and H_2O, consistent with complete combustion of the cyclopentadienyl (Cp) ligands on the organocobalt compound. Based on the growth rate for ALD cobalt oxide of 2.2 Å/cycle determined on planar surfaces and the AAO geometry, we estimate a Co loading for the ALD catalysts of 0.8 wt% (1.5×10^{-4} g Co).

The size-selected cobalt cluster-based catalysts (Co_{17-33}/Al_2O_3/ZnO/Al_2O_3/AAO) were prepared by depositing a narrow size-distribution of cobalt clusters generated in a laser vaporization cluster source as illustrated in Fig. 2. The ZnO inter-

Author's personal copy

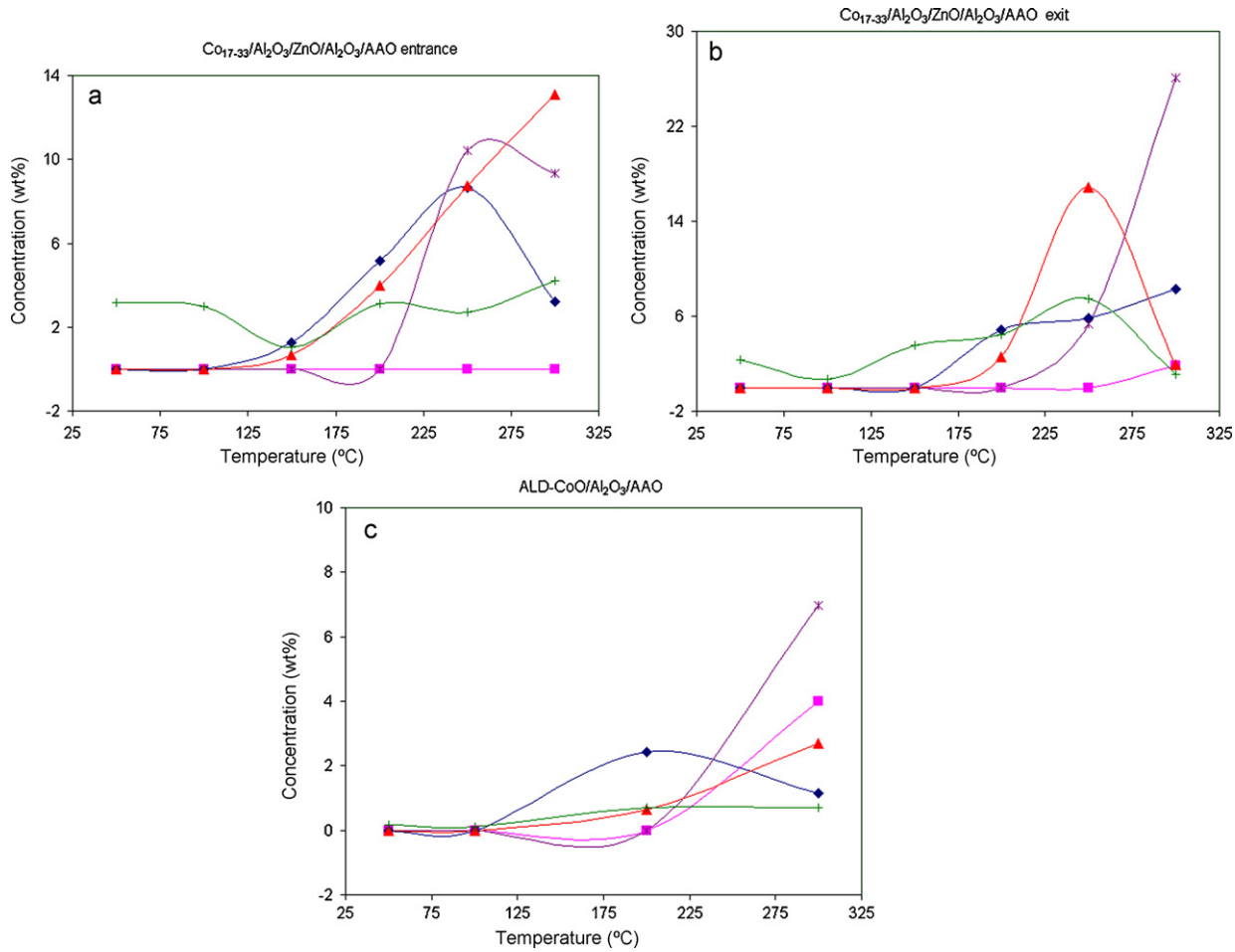

Fig. 4. Concentration of condensed products vs. reaction temperature in oxidative decomposition of 1-methoxy-2-methyl-2-propanol (MMP) over various catalysts. C_1 – methanol (+); C_3 – acetone (▲) and C_4 – 1,2-butanediol (◊), 3-hydroxy-2-butanone (*) and 2,3-butanedione (■) on: size pre-selected cobalt clusters at the entrance (a), exit (b) of the channels of the AAO membrane, and ALD-coated catalyst (c) as a function of temperature.

layer between the two alumina layers assures conductivity of the AAO support for measuring the flux of charged cluster ions during deposition. It does not change surface property of Al_2O_3 layer. The size selected cluster deposition method was described elsewhere [25,26,28]. In brief, cobalt clusters were prepared by laser vaporization of a cobalt target. The cluster beam was confined in a quadrupole ion guide assembly and Co_{17-33} clusters selected by operating the quadrupole deflector as energy filter. The deposited amount of cobalt cluster was determined by on-line monitoring of the deposition flux. The formation of multiply charged ions in this kind of source is negligible. The cobalt loading on the AAO was equivalent to 77% of a close-packed Co monolayer (ML), covering two 3-mm diameter spots on the AAO membrane. This corresponds to 21 ng of cobalt metal. From X-ray absorption near edge spectroscopy (XANES, not shown), the oxidation states of Co for both ALD-prepared and cluster deposition-prepared catalysts are similar, the best resembling Co (II), as compared to reference materials cobalt nitrate and cobalt oxide [32].

Table 1
Reactivity of cobalt catalysts in oxidative decomposition of 1-methoxy-2-methyl-2-propanol (MMP).

Catalyst	Cobalt loading (g)	COx selectivity (%)	Product turn over rate (s^{-1})[a]				
			Methanol	Acetone	1,2-Butanediol	3-Hydroxy-2-butanone	2,3-Butanedione
$Co_{17-33}/Al_2O_3/ZnO/Al_2O_3/AAO$ (at the gas exit of the membrane channels)	2.1×10^{-8}	0	137	123	280	970	81
$Co_{17-33}/Al_2O_3/ZnO/Al_2O_3/AAO$ (at the gas entrance of membrane channels)	2.1×10^{-8}	1	505	869	62	241	0
1 ALD-cycle $CoO/Al_2O_3/AAO$ (uniformly coated)	1.5×10^{-4}	4	0.01	0.02	0	0.02	0.02

Reaction conditions: Temperature: 300 °C; 4% MMP–2% O_2–4% H_2O–He; total flow rate: 30 ml/min. The activity data shown are background corrected – after the subtraction of the activity of the blank alumina-coated AAO measured under the identical reaction conditions.

[a] Turn over rates per cobalt atom, calculated based on total cobalt loading.

Author's personal copy

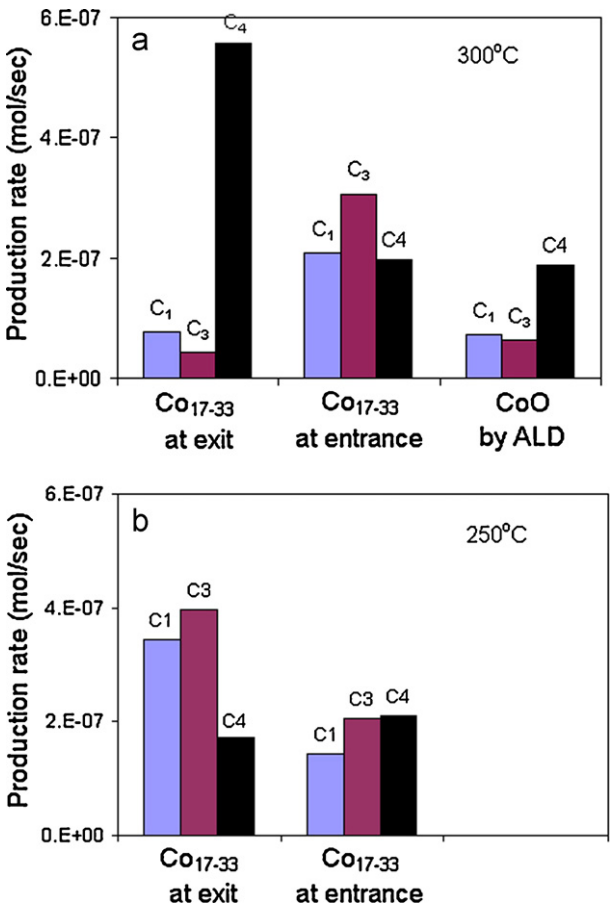

Fig. 5. Products formed at 300 °C (a) and 250 °C (b). C_1: carbon dioxide and methanol; C_3: acetone; C_4: 1,2-butanediol, 3-hydroxy-2-butanone, and 2,3-butanedione. In addition to the formation rates on size-selected clusters positioned at the entrance (long contact time) and exit (short contact time) of the membrane, the rate for the ALD-coated membrane is shown as well. Note, that the ALD-coated membranes are coated uniformly with the catalyst, thus reversing gas flow has no effects on contact time. The rates are shown as measured, without normalization to the metal loading.

2.3. Catalytic testing

The oxidative MMP decomposition reactions were conducted under steady-state conditions. A quartz tube (O.D. = 1 in. for the top and O.D. = 1/4 in. for the bottom) with a porous quartz frit supporting the catalytic AAO membrane (O.D. = 3/8 in., Al ring O.D. = 3/4 in.) was used as a packed-bed flow reactor. One membrane was used per test. The estimated Co loadings on membranes by ALD and by cluster deposition are listed in Table 1 and were discussed in Section 2.2. The MMP surrogate with a boiling point of 115 °C was introduced into stream of the carrier gas by a calibrated syringe pump (Kd Scientific) and vaporized in the heated gas feed line before entering the reactor. The reaction was conducted at atmospheric pressure using a gas mixture of 4% MMP, 2% O_2 and 4% H_2O balanced by He at a total gas flow rate of 30 ml/min. The gas feed direction was from the top to bottom of the catalyst membrane (see Fig. 6). During the temperature ramp (50–300 °C, step 50 °C), at each temperature the reaction was conducted for 1 h. The temperature conditions were based on the result that MMP does not decompose at 300 °C. The liquid reaction products and the unreacted fraction of MMP collected at the exit of the reactor in a condenser and subsequently analyzed by a gas chromatograph equipped with mass spectrometer (GC–MS: HP 5970/6890). An online HP-5890 gas chromatograph (GC) equipped with a thermal conductivity detector (TCD) was used to quantify the gas phase products. The cobalt catalysts were used as prepared (oxidized) and no pretreatment of the catalysts was performed before the tests. A blank test on Al_2O_3/AAO membrane was also done and the results in Table 1 were already subtracted by the blank.

3. Results and discussion

A condenser was placed after the reactor exit and before the GC. Most of the products were collected in this condenser in the liquid phase. CO and CO_2 were identified as main gas phase products by online GC analysis, The oxygen conversions in all three Co catalyst testings were ~75% at 300 °C but the selectivity to CO and CO_2 was 22% for ALD-prepared catalyst and 18% for cluster deposition-prepared catalyst. On the alumina support itself, the O_2 conversion was 43% and the COx selectivity was 17%. Co catalysts did increase the oxygen conversion while the COx selectivity did not change much. The results in Table 1 were subtracted by the blank support. The GC–MS analysis of the condensed liquid phase identified methanol, acetone, 1,2-butanediol, 3-hydroxy-2-butanone, and 2,3-butanedione as major reaction products. As shown in the schematics in Fig. 3, the disappearance of methoxy group indicates the cleavage of the targeted C–O–C bond. The presence of methanol implies that the hydrolysis reaction is taking place. Alcohol dehydration pathway is not favorable under these conditions since the reaction feed includes 4% H_2O. 1,2-butanediol can form via C–O–C bond cleavage, followed by hydrolysis, and methyl group rearrangement. 3-Hydroxyl-2-butanone production can take place by the C–O–C cleavage, followed by hydrolysis, methyl migration, and –C–OH bond oxidation steps. A further oxidation is needed to the formation of 2,3-butanedione. The lack of C_2 products indicates a high stability of the C_3 compounds and the absence of a reaction path for recombination reaction from C_1 (CH_x) species. Acidic aluminas are known to catalyze the hydrolysis reaction, for example, dimethyl ether. However, the AAO membrane substrate in this study is not the active catalytic component for ether cleavage because results from blank tests for AAO membrane show the very low activity. The different selectivity of ALD-CoO sample is due to the homogeneous covering of CoO layer on the alumina substrate during the deposition step. The first set of hydrolysis products should be methanol and 2-methyl-1,2-propanediol. The lack of the latter by GC–MS identification indicates the isomerization of 2-methyl-1,2-propanediol to 1,2-butanediol (A). Products B and C are indeed derivative products by further oxidation of A.

Fig. 4 summarizes the results of the analysis of the C_1–C_4 liquid product fraction over the size-selected cluster-based cobalt catalyst with clusters at the entrance (Fig. 4(a)) and clusters at the exit of the membrane channels (Fig. 4(b)) along with the results for the ALD-cobalt catalyst (Fig. 4(c)), over the temperature range of 50 °C to 300 °C. It appears that the oxidizing conditions were mild, since 3-hydroxy-2-butanone had the highest concentration in all three cases as one of the primary C_4 products while 2,3-butanedione (over-oxidized product) concentration was very low. Compared to the cluster-based catalysts, the ALD prepared catalyst with cobalt oxide throughout the pores, had considerably lower activity (Fig. 4(c)).

The activity of the size-selected clusters was identical for the clusters positioned at the entrance or at the exit of the membranes, both producing only a negligible amount of 2,3-butanedione. However the selectivity-temperature profile towards other products is very different. With clusters placed in the gas entrance position, the other two C_4 products (1,2-butanediol and 3-hydroxy-2-butanone) had maximum production at 250 °C, while at 300 °C their production dropped (Fig. 4(a)) at the expense of C_1 (methanol) and C_3 (acetone) formation. When the clusters were placed at the gas exit position (Fig. 4(b)), the results were reversed, with C_4 products

Author's personal copy

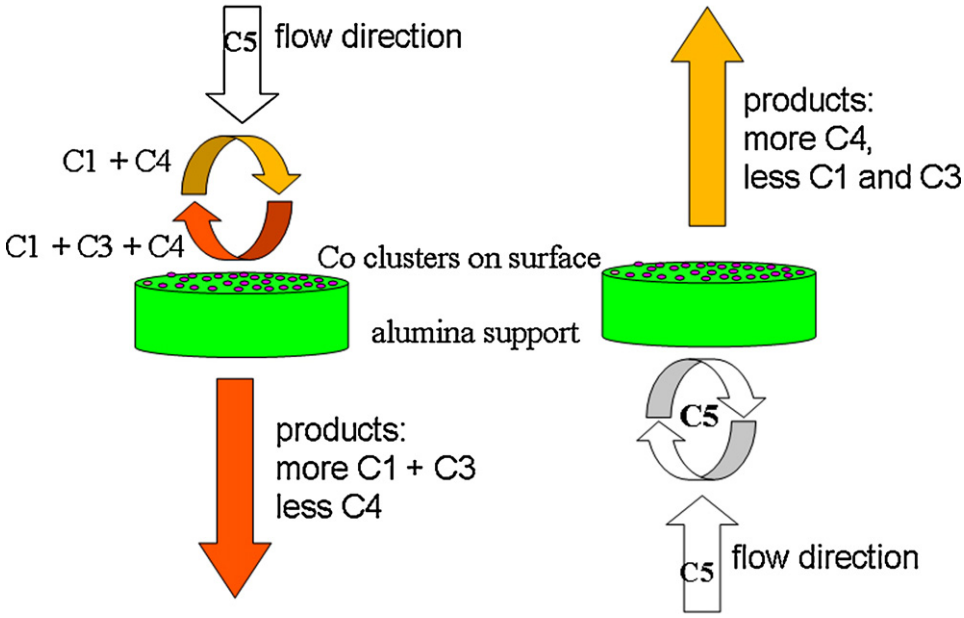

Fig. 6. Schematic of the catalyst testing of the $Co_{17-33}/Al_2O_3/ZnO/AAO$ sample in two geometries with respect to the gas flow: with catalytic particles (dots) located at the entrance of the membrane, thus higher number of collisions/longer contact time (left panel) and at the exit of the membrane corresponding to shorter contact time (right panel). The arrows represent the reactant gas flow direction.

keeping increasing with temperature whereas C_1 and C_3 production leveled off at 250 °C. The strongly temperature and position (contact-time) dependent selectivity of the size-selected clusters is compared in Fig. 5.

In Figs. 4 and 5, one may notice the low C_1 selectivity in comparison with the C_3 and C_4 products. Basically, if the mechanism is to follow a simple decomposition path of $C_5 \rightarrow C_1 + C_4 \rightarrow C_1 + (1-x)\,C_4 + x(C_1 + C_3) \rightarrow (1+x)\,C_1 + (1-x)\,C_4 + xC_3$, then the mole ratio of C_1 should be equivalent to $C_3 + C_4$. Presumably, the apparent loss of C_1 resulted from carbon deposits on the membrane. This assumption was confirmed by the color change of the membranes during reaction. The initial color of the catalyst is light brownish. After reaction, the color changed to dark (black). We have evidence from SEM (not shown) to confirm significant carbon deposition on the membranes took place during reaction (coke formation). It was also seen on the substrate-alumina AAO membrane itself. We attribute the dark color that appears after testing to carbon.

In addition to the well defined size and precise loading of the nanocatalysts, cluster deposition possesses another advantage, namely exact control of the location of the catalytic particles at the entrance or at the exit of the nanochannels of the AAO membrane. This feature enables straightforward studies of the effect of the contact time (i.e. number of collisions of the reactants, intermediates and products with a catalytic particle) on catalytic activity and fine-tuning of the selectivity of the catalysts. Fig. 6 shows the two gas flow patterns for clusters positioned at the entrance – many collisions = longer contact time (a) or at the exit – limited number of collisions = shorter contact time) (b) of the membrane channels. In case (a), only a small part of the gas flow can make its way through the membrane pores at once, while most of the backflow will make contact again. This will lead to a situation where the cobalt oxide clusters have a higher number of collisions and longer contact time [33]. The potential readsorption of the primary products on the catalyst may give rise to secondary products. In case (b), when the reactant gas reaches the catalyst after already passing the pore a dominant formation of primary reaction products is expected, with a low probability of readsorption. The significant effect of the contact time on the outcome of the reaction on size-selected clusters is summarized in Fig. 5(a and b), with superior selectivity at 300 °C of the cobalt clusters toward C_4 at the exit of the pores.

In order to determine per metal activity of the cluster- and ALD-based catalysts, the product formation rates were normalized to the total cobalt loadings applied. The amount of cobalt loading from cluster deposition corresponds to 21 (±2) ng (equivalent to $\sim 2 \times 10^{-6}$ wt% loading), which is 4 orders of magnitude lower than that of the ALD-coated sample. The calculated turn-over rates (TOR) are summarized in Table 1. These calculations assume that all of the ALD cobalt oxide catalytic sites are sampled equally by the MMP. It is likely that catalytic sites deep within the high aspect ratio AAO pores are sampled infrequently due to transport limitations. Consequently, the TOR values for the ALD cobalt oxide in Table 1 represent lower limits. As far as the comparison of reactivity considered, the sub-nanometer size cobalt catalysts posses a per atom activity by 4–5 orders higher than the sample uniformly coated ALD cobalt oxide. The most likely cause of the higher activity of the cluster-based catalysts is the fact that these subnanometer sized particles consist of a large fraction of under-coordinated surface atoms. Interestingly, the total activity of the subnanometer clusters while at the exit or the entrance of the membrane was identical within the experimental error. This indicates that only subnanometer clusters in the pores of the membranes are active under our reaction conditions, while larger cobalt aggregates, that at the coverage applied are expected to form on the flat surface [34] of the membrane, posses no or only negligible activity and have the role of spectators only.

In addition to the high activity of the cobalt clusters, at a practically complete lack of combustion, the selectivity of the cluster-based sample towards longer vs. shorter C_x products can be readily tuned via controlling the contact time (i.e. number of collisions) by simply placing the catalytic particles on the exit vs. entrance of the membrane with respect to the flow. This observation, which is contrary to the behavior of subnanometer Pt clusters in the oxidative dehydrogenation of propane [25] most likely reflects comparable activation energies for the activation of various bonds in the surrogate on the subnanometer cobalt clusters. The indifference of Pt routed in the very low activation

Author's personal copy

barrier of breaking the C–H bond in comparison with any other bond in propane explains why there was no change with position, i.e. contact time/number of collisions of propane and intermediates/products with the cluster. Cobalt oxide species seems to be different in the MMP study. Having clusters at the entrance causes deeper breakdown, i.e. higher fraction of shorter chains. Thus, it is likely the barriers are comparable for various bonds in MMP.

4. Conclusions

Cobalt based catalysts can catalyze the oxidative decomposition of MMP, a model compound for cellulose. Reaction products indicates the C–O–C bond cleavage by hydrolysis, as well as the subsequent steps of methyl group migration, and/or –C–OH oxidation to –C=O. Subnanometer size-selected Co clusters produced by cluster deposition have 4–5 orders of magnitude higher turn-over rates than the cobalt oxide prepared by atomic layer deposition. Furthermore, the high selectivity of the small clusters can be readily controlled by temperature and position of the clusters on the membrane with respect to the gas flow. Only a small fraction of the feedstock (<18%) is combusted on these catalysts compared to 17% combusted on alumina support.

Acknowledgement

This work was supported by the US Department of Energy, BES-Chemical Sciences under contract FWP 57703, BES Materials Sciences and BES-Scientific User Facilities under contract DE-AC-02-06CH11357 with UChicago Argonne, LLC, Operator of Argonne National Laboratory.

References

[1] P.L. Dhepe, A. Fukuoka, Catal. Surv. Asia 11 (2007) 186–191.
[2] J. Schurz, Prog. Polym. Sci. 24 (1999) 481–483.
[3] A. Fukuoka, P.L. Dhepe, Angew. Chem. Int. Ed. 45 (2006) 5161–5163.
[4] L.T. Fan, M.M. Gharpuray, Y.-H. Lee, Cellulose Hydrolysis (1987).
[5] W.S. Mok, M.J. Antal, G. Varhegyi, Ind. Eng. Chem. Res. 31 (1992) 94–100.
[6] Y.-H.P. Zhang, L.R. Lynd, Biotechnol. Bioeng. 88 (2004) 797–824.
[7] J.R. Peter, Starch – Stärke 51 (1999) 269–274.
[8] M. Marzorati, B. Danieli, D. Haltrich, S. Riva, Green Chem. 7 (2005) 310–315.
[9] M. Asadullah, K. Fujimoto, K. Tomishige, Ind. Eng. Chem. Res. 40 (2001) 5894–5900.
[10] R. Gopinath, A.R. Paital, B.K. Patel, Tetrahedron Lett. 43 (2002) 5123–5126.
[11] E. Roduner, Nanoscopic Materials: Size-Dependent Phenomena, The Royal Society of Chemistry, Cambridge, 2006.
[12] M. Valden, X. Lai, D.W. Goodman, Science 281 (1998) 1647–1650.
[13] J.M. Ramallo-López, F.G. Requejo, A.F. Craievich, J. Wei, M. Avalos-Borja, E. Iglesia, J. Mol. Catal. A: Chem. 228 (2005) 299–307.
[14] E. Bus, R. Prins, J.A. van Bokhoven, Catal. Commun. 8 (2007) 1397–1402.
[15] Q. Fu, H. Saltsburg, M. Flytzani-Stephanopoulos, Science 301 (2003) 935–938.
[16] A.A. Herzing, C.J. Kiely, A.F. Carley, P. Landon, G.J. Hutchings, Science 321 (2008) 1331–1335.
[17] B. Yoon, H. Häkkinen, U. Landman, A.S. Wörz, J.-M. Antonietti, S. Abbet, K. Judai, U. Heiz, Science 307 (2005) 403–407.
[18] M.A. Rottgen, S. Abbet, K. Judai, J.M. Antonietti, A.S. Worz, M. Arenz, C.R. Henry, U. Heiz, J. Am. Chem. Soc. 129 (2007) 9635–9639.
[19] S. Lee, C. Fan, T. Wu, S.L. Anderson, J. Am. Chem. Soc. 126 (2004) 5682–5683.
[20] W.E. Kaden, T.P. Wu, W.A. Kunkel, S.L. Anderson, Science 326 (2009) 826–829.
[21] L.D. Socaciu, J. Hagen, J. Le Roux, D. Popolan, T.M. Bernhardt, L. Woste, S. Vajda, J. Chem. Phys. 120 (2004) 2078–2081.
[22] J. Hagen, L.D. Socaciu-Siebert, J. Le Roux, D. Popolan, S. Vajda, T.M. Bernhardt, L. Woste, Int. J. Mass Spectrom. 261 (2007) 152–158.
[23] T.M. Bernhardt, Int. J. Mass Spectrom. 243 (2005) 1–29.
[24] R.C. Bell, K.A. Zemski, A.W. Castleman, J. Clust. Sci. 10 (1999) 509–524.
[25] S. Vajda, M.J. Pellin, J.P. Greeley, C.L. Marshall, L.A. Curtiss, G.A. Ballentine, J.W. Elam, S. Catillon-Mucherie, P.C. Redfern, F. Mehmood, P. Zapol, Nat. Mater. 8 (2009) 213–216.
[26] S. Lee, L.M. Molina, M.J. López, J.A. Alonso, B. Hammer, B. Lee, S. Seifert, R.E. Winans, J.W. Elam, M.J. Pellin, S. Vajda, Angew. Chem. Int. Ed. 48 (2009) 1467–1471.
[27] S. Vajda, S. Lee, K. Sell, I. Barke, A. Kleibert, V. von Oeynhausen, K.-H. Meiwes-Broer, A.F. Rodriguez, J.W. Elam, M.M. Pellin, B. Lee, S. Seifert, R.E. Winans, J. Chem. Phys. 131 (2009) 121104.
[28] Y. Lei, F. Mehmood, S. Lee, J. Greeley, B. Lee, S. Seifert, R.E. Winans, J.W. Elam, R.J. Meyer, P.C. Redfern, D. Teschner, R. Schlogl, M.J. Pellin, L.A. Curtiss, S. Vajda, Science 328 (2010) 224–228.
[29] L. M. Molina, S. Lee, K. Sell, G. Barcaro, A. Fortunelli, B. Lee, S. Seifert, R. E. Winans, J. W. Elam, M. J. Pellin, I. Barke, A. Kleibert, V. von Oeynhausen, Y. Lei, R. J. Meyer, J. A. Alonso, A. Fraile-Rodríguez, S. Giorgio, C. R. Henry, K.-H. Meiwes-Broer and S. Vajda Catal. Today, (2010) in press, doi: 10.1016/j.cattod.2010.08.022.
[30] S. Lee, B. Lee, F. Mehmood, S. Seifert, J.A. Libera, J.W. Elam, J. Greeley, P. Zapol, L.A. Curtiss, M.J. Pellin, P.C. Stair, R.E. Winans, S. Vajda, J. Phys. Chem. C. 114 (2010) 10342–10348.
[31] J.W. Elam, M.D. Groner, S.M. George, Rev. Sci. Instrum. 73 (2002) 2981–2987.
[32] S. Lee, B. Lee, S. Seifert, R.E. Winans, J.A. Libera, J.W. Elam, M.J. Pellin, S. Vajda (in preparation).
[33] S.E. Albo, L.J. Broadbelt, R.Q. Snurr, AiChe J. 52 (2006) 3679–3687.
[34] T. Hill, M. Mozaffari-Afshar, J. Schmidt, T. Risse, S. Stempel, M. Heemeier, H.J. Freund, Chem. Phys. Lett. 292 (1998) 524–530.